Fine-Tuning the Degree of Stem Cell Polarization and Alignment on Ordered Arrays of High-Aspect-Ratio Nanopillars

Michael A. Bucaro,‡ Yolanda Vasquez,‡ Benjamin D. Hatton,‡ and Joanna Aizenberg*

School of Engineering and Applied Sciences, Wyss Institute for Biologically Inspired Engineering, and Kavli Institute for Bionano Science and Technology, Harvard, Harvard University, 29 Oxford Street, Cambridge, Massachusetts 02138, United States. ‡These authors contributed equally.

ABSTRACT

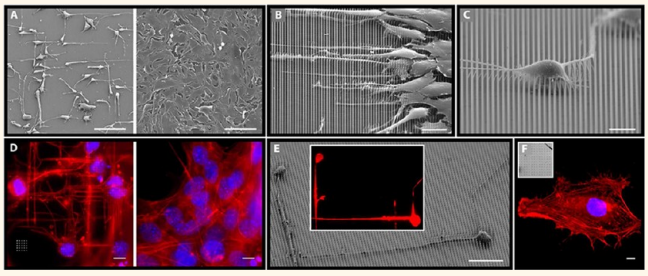

Nanobiomaterials are introducing new capabilities to coordinate cell selection, growth, morphology, and differentiation. Herein, we report that tuning the geometry of ordered arrays of nanopillars (NP) elicits specialized morphologies in adherent cells. Systematic analysis of the effects of the NP radius, height, and spacing reveals that stem cells assume either flattened, polarized, or stellate morphologies in direct response to interpillar spacing. Notably, on NPs of pitch near a critical spacing ($d_{crit} \approx 2\ \mu$m for C3H10T1/2 cells), cells exhibit rounding of the cell body, pronounced polarization, and extension of narrow axon-like cell projections aligned with the square lattice of the NP array and extending hundreds of micrometers. Furthermore, increasing the NPs' aspect ratio from 12:1 to 50:1 to produce NPs with a corresponding reduction in the NP bending stiffness of 2 orders of magnitude amplified the cellular response and resulted in a previously unseen degree of cell polarization and alignment. The rapid morphological transformation is reproducible on surfaces that maintain key parameters of the NP geometry and spacing, is influenced by the cell seeding density, and persists for different stem cell lines and primary mesenchymal stem cells. The demonstrated ability to support various morphogenetic trends in stem cells by simply tuning the geometry of the NP substrates provides a stepping-stone for the future design of scaffolds where cellular morphology and alignment are crucial.

KEYWORDS: C3H10T1/2 cells · nanopillar arrays · stem cell morphology · cell alignment

Manipulation of cell fate on biomaterials is a fundamental goal of regenerative medicine.[1−5] Next-generation solutions include implantable materials that will actively participate in tissue formation. This can be achieved by programming multiple cell-instructive cues into the biomaterial itself.[3−13] For example, biomaterials can release growth factors, present ligands, and deliver physical cues in order to sequentially recruit, organize, and differentiate stem cell populations.[4,6,10,13−17] These smart biomaterials can also provide transformative tools for probing the mechanisms that instruct cell behavior and biosensing applications.[9,18−20] The architecture of the biomaterial surface is a critical element in controlling cell behavior through contact guidance[11,21−23] and is the foundation from which physical and chemical extracellular signals that are essential to defining phenotype are presented to cells (*i.e.*, adhesion ligands and material elasticity).[23−25] Experiments over the last several decades have shown that topographic cues, initially at the microscale and more recently at the nanoscale, can influence the behavior and differentiation of various cell types.[9,10,12,15−22,26−29] There is enormous potential to utilize substrate topography, particularly in applications where cell polarity and organization are required.[30] For instance, in neuroelectronics, topography could be used to control the directionality of neurite growth and define the polarity of neuronal junctions. Identification of topographies that elicit specific cellular responses, and understanding how cells interpret these topographic cues, will enable the design of "smart" materials that use topography to present chemical, mechanical, and other vital cell stimuli.

Cell morphology is a critical gauge of a material's performance. Cell shape influences expression profiles, signaling pathways that guide differentiation, and is an indicator of normal function in most cell types.[25,31−33] Numerous studies of cell growth on flat substrates have demonstrated that cell morphology is extremely responsive to spatial restrictions, adhesion site availability

* Address correspondence to jaiz@seas.harvard.edu.

Received for review April 15, 2012 and accepted June 20, 2012.

Published online June 20, 2012
10.1021/nn301654e

and distribution, substrate elasticity, and topographical order.[9,11,18,21,24,28,34−36] An increasing number of studies highlight the sensitivity of morphology and gene expression to micro- and nanoscale grooves, pillars, or pits.[9,12,18−21,24,27−29,34−38] For example, oriented fibroblast growth was previously demonstrated on nanoblades, and rounding of cells was reported on nanopillars (NPs).[39] Various studies have also developed polymeric micropillar arrays for quantitative measurements of cellular forces.[18,29,40−42] These reports demonstrate that micro- and nanotopographies, particularly NP arrays, could provide a basis for several levels of functionality on biomaterial surfaces. These isolated studies do not, however, systematically study the effect of combinations of geometry, spacing, and stiffness of NPs on cell shape and differentiation.

We have previously demonstrated several of the design elements for creating NP-based programmable biomaterials including mechanical actuation of NPs and tuning NP mechanical stiffness.[43−49] NPs can be chemically functionalized,[46,50] patterned, electrically addressed, and actuated.[45,49] Patterned NP arrays can be fabricated by photolithography in silicon, replicated into polymers by molding, or produced by a variety of other techniques including growth of carbon or metal oxide nanowires to provide a diversity of chemical and physical properties.[43,47,48] In particular, spatial confinement and adhesion site availability for cell attachment can be controlled by varying NP size and interpillar spacing.[51] Importantly, the elasticity of the substrate and its influence on cell differentiation can also be controlled *geometrically* by changing the radius and length of the NPs in addition to using a different material with a different Young's modulus, thus enabling the use of materials that provide other essential characteristics while achieving a tunable elasticity on the surface.

Here, we systematically scrutinize the influence of various geometries, geometry-induced elasticity, and densities of ordered NP arrays on the morphology of pluripotent cells. Specifically, we focus on the mesenchymal progenitor cell line C3H10T1/2 since it is a model of differentiation to several lineages, which include adipocytes, osteocytes, and chondrocytes, among others. We find that stem cell shape and alignment can be finely tuned as a function of the NP spacing and geometry. We have identified a characteristic spacing for stem cells (~2 μm) using high-aspect-ratio (geometrically soft) NPs that induce dramatic polarization and growth of axon-like extensions that align with the NP lattice. We believe that ultimately this NP platform can deliver not only topographic but also chemical and physical stimuli and dynamically change these parameters through actuation and, thus, provides a powerful tool for attracting desired cell populations, programming their shape, and directing their fate.

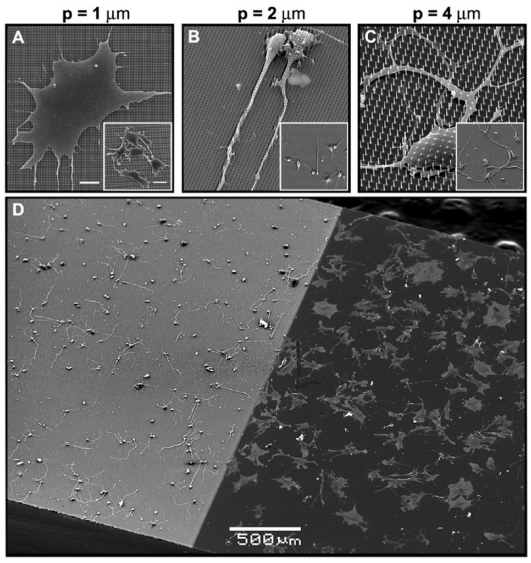

Figure 1. C3H10T1/2 cells grown for 1 day on NP arrays with a spectrum of NP spacings. Representative SEM images of cells on arrays of 1 μm (A), 2 μm (B), and 4 μm pitch (C) show different stem cell morphologies as a function of NP density. Insets are lower magnification images. (A) Cells grown on regions with p = 1 μm spread similarly to cells on polished silicon. (B) A dramatic change to neuron-like morphologies occurs at p = 2 μm. The majority of cells develop a single extension spreading across the NPs. (C) Cells on NPs of p = 4 μm extend past the NPs and spread at the bottom of the surface and develop multiple, highly branched extensions. (D) Image of cells grown on a substrate having a 2 μm pitch NP region (left) and adjacent unetched, flat region (right); note profoundly different, highly uniform, and statistically significant morphological trends with highly polarized cells on the NP. Scale bars (A, B, C) 10 μm, insets 20 μm, (D) 500 μm. See also Figure S1.

RESULTS

Silicon nanopillars patterned in square-lattice arrays with a gradient of interpillar spacings (pitch) were fabricated with a NP aspect ratio of 12:1 (diameter of 400 nm, length of 5 μm, pitch changing from 0.8 to 5 μm). Mouse embryo-derived stem cells (C3H10T1/2) were cultured on the gradient NP arrays as well as NP arrays with a constant pitch of 1, 2, or 4 μm for 1 day, and their morphology was assessed by optical microscopy and scanning electron microscopy (SEM).[52] Distinct morphological characteristics were observed as a function of the pitch of the NP arrays. Figure 1 shows SEM images of representative cells grown on NP arrays of 1, 2, and 4 μm pitch (see also Figure S1). The characteristic spindle-shaped morphology of this cell line was maintained on polished silicon (flat) as well as on the region of the gradient sample with small interpillar spacings ranging from 0.8 to 1.25 μm. Similarly, on 1 μm constant-pitch NPs, cells were broad with high projected cell area (Figure 1A). On these densely packed NP arrays, the cells were characteristically adherent to the tips of the NPs and did not penetrate significantly between the NPs. With increasing NP pitch, obvious changes in cell morphology were noted. On a gradient sample of NPs with 1.5−2.5 μm spacing

TABLE 1. Morphological Differences among C3H10T1/2 Cells Cultured on Flat Si and 12:1 Aspect Ratio NPs with Varying Pitch

sample	% cells polarized (SD)	projected area/cell, μm^2 (SD)	general morphology
flat silicon	20 (12.0)	475.6 (126.3)	spindle-shaped, flattened
NP, $p = 1$ μm	32.7 (4.7)	236.1 (37.8)	spindle-shaped, flattened
NP, $p = 2$ μm	70.2 (11.0)[a]	92.4 (38.8)[a]	highly polarized
NP, $p = 4$ μm	66.6 (6.2)[a]	263.3 (63.6)	stellate, highly branched

[a] Significant difference relative to flat Si and NP with $p = 1$ μm.

TABLE 2. Number of Extensions Grown by C3H10T1/2 Cells on Flat Si and 50:1 Aspect Ratio NPs with $p = 2$ μm

extentions per cell	% cells (SD) on flat Si	% cells (SD) on flat Si
0	49.5 (4.8)	23.3 (3.2)[a]
1	32.6 (0.7)	56.7 (4.1)[a]
2	13.6 (7.2)	15.2 (4.0)
≥3	4.3 (4.4)	4.8 (3.1)

[a] Significant difference relative to flat Si.

and on 2 μm constant-pitch NPs cells exhibited rounded cell bodies and long narrow extensions (Figure 1B). In striking contrast to the flattened morphology of cells on a higher density NP or polished silicon, the morphology of nearly all cells on a 2 μm constant pitch sample was characteristic of three-dimensional cultures or neuronal cells *in situ* (Figure 1D). The cells remained largely suspended on the NPs and grew long, narrow axon-like extensions that bridged the NPs and rarely contacted the underlying substrate. In regions with a pitch of ~3.5−5 μm on the gradient sample and on the 4 μm constant-pitch substrate, the cells assumed a stellate morphology and grew multiple cell extensions with increased branching relative to cells on 2 μm pitch NPs. The cells consistently penetrated beyond the NPs and onto the underlying substrate (Figure 1C). Image analysis of fluorescently labeled cells (see Methods) showed that the vast majority of cells on both 2 and 4 μm pitch NPs were morphologically polarized and that the projected cell area was reduced 5-fold in cells on 2 μm pitch NPs relative to cells on polished silicon (Table 1). Image analysis of 1 day cultures indicated the majority of cells on the 2 μm pitch NPs had a single dominant extension, a significant increase relative to cells on polished silicon in which the largest population had no significant extensions (Table 2). The majority of cell extensions bridged NPs in the ⟨10⟩ lattice direction along the principal axes of the NP array, significantly greater than extending in all other lattice directions, with the second highest frequency in the diagonal ⟨11⟩ direction (Table 3).

The striking transformation in cell morphology observed on NPs of 2 μm pitch is consistent with a neuronal phenotype and, therefore, may be useful for

TABLE 3. Alignment of Extensions of C3H10T1/2 Cells with Lattice Directions of NPs with $p = 2$ μm

lattice direction	% cells segments	SD
<10>	65.8	14.4
<11>	15.6	6.3
<21>	9.6	6.1
<31>	6.3	3.2

neuronal engineering applications. We therefore evaluated this spacing further with regard to (i) the NP aspect ratio (which will correspond to the effective change of surface elasticity), (ii) surface chemistry, and (iii) cell seeding density. Cell growth was evaluated on NP substrates with 2 μm pitch and aspect ratios of 1:12 (diameter = 400 nm, height = 5 μm) and 1:50 (diameter = 200 nm, height = 10 μm). These modest changes in geometry produce a 128-fold decrease in NP bending stiffness (from calculated values of 100 nN/nm to 1 nN/nm) according to the following expression relating the bending stiffness of cantilevers of differing geometry:

$$\frac{S_{1effect}}{S_{2effect}} = \left(\frac{E_1}{E_2}\right)\left(\frac{l_2}{l_1}\right)^3\left(\frac{r_1}{r_2}\right)^4$$

The changes in geometry were further confirmed by direct AFM measurements.[43] We observed that fluorinated surfaces promoted cell growth on the NP tips and minimized cell interactions with the underlying substrate; therefore, we conducted the following studies on NPs treated with a self-assembled monolayer of fluorinated silane.

Cells were seeded at a density of 5×10^4 cells/cm^2 and cultured for 1 day on the NPs of aspect ratio 1:12 and 1:50. Both optical and SEM analysis showed that cells exhibited similar rounded cell bodies and axon-like extensions on all 2 μm pitch surfaces (Figure 2). Notably however, the geometrically softer, high-aspect-ratio NP arrays induced more prominent cell polarization and the alignment of cell extensions with the orientation of the underlying NP square-lattice array, while cells on the adjacent polished silicon spread broadly and radially uniformly and expanded to confluency over 1 day (Figure 2A). The morphology of the cells on the NPs was dependent on cell seeding density (Figure S2). At high cell seeding density (5×10^6 cells/cm^2) cells were confluent on the NP array and cell elongation was minimal. This is demonstrated by cells seeded in dispersed aggregates that grow axon-like processes only at the peripheries where cells extend uninterrupted across the nanopatterned surface (Figure 2B). Cell bodies characteristically rested atop the NPs with extensions that traversed the NPs (Figure 2C; Figure S2). To demonstrate that it is the pseudo-3D structure of the "soft" NPs that guides the morphological transformation and that the simple distribution of chemically adhesive patches on the flat

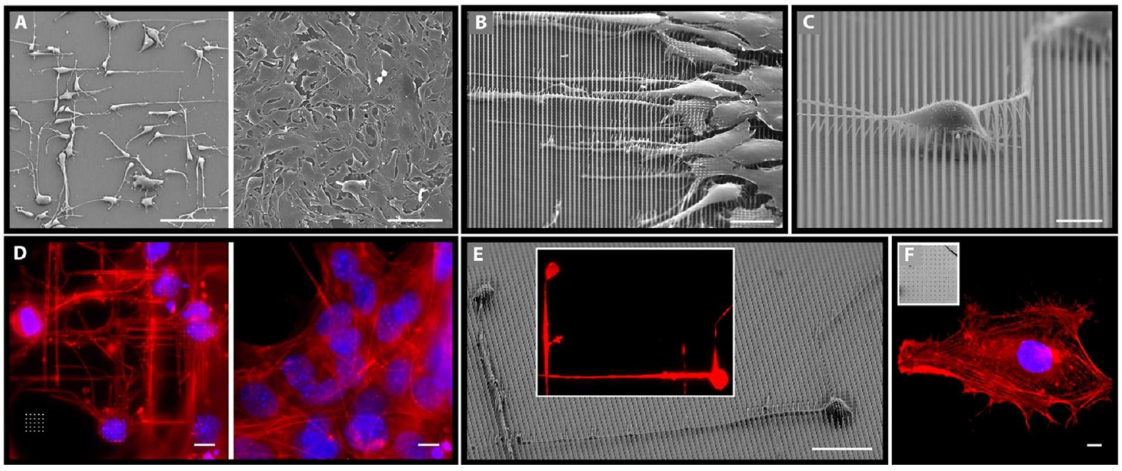

Figure 2. Oriented growth and polarization of C3H10T1/2 cells by high-aspect-ratio, "geometrically soft" NPs. (A) SEM images of C3H10T1/2 cells after 1 day of culture on NPs of l = 10 μm, r = 100 nm, p = 2 μm (left) and unetched/polished silicon wafer (right) for cell seeding density of 5 $\times$ 10^5 cells/cm^2. On the NP array, the cells are highly polarized and aligned with the NP grid (⟨10⟩ direction of square NP lattice is aligned with the edges of the image). (B) SEM showing oriented cell extensions at the edge of a cell aggregate after 1 day of culture (see also Figure S2). (C) SEM of a cell on NPs taken from a shallow angle showing the cell resting on the tips of NPs. (D) Optical images showing actin cytoskeleton (red) and nuclei (blue) of cells after 2 days of culture on NPs (left) and polished silicon (right). (E) SEM and live cell optical image (inset) of the same cells stained with R18 after 1 day of culture on NPs (see also Figures S2,3). (F) Optical image of actin (red) and nuclei (blue) of a cell on a flat sample with a 2D array of adhesion sites (inset at same magnification). Scale bars: 100 μm (A), 20 μm (B, E), 10 μm (C, D, F).

surface at the same distances as our substrates has no pronounced effect on cell polarization, C3H10T1/2 cells were cultured for 1 day on flat surfaces with 2D patterns of adhesion sites (FN), which were created using the same lithographic mask as the NP arrays. The cells spread broadly, similar to cells on polished silicon, showing no polarization or alignment with the underlying 2D patterns (Figure 2F).

Evaluation of the actin cytoskeleton by fluorescence microscopy after 2 days in culture on high-aspect-ratio NP arrays further demonstrated the strong preference for alignment of the cell apparatus with the directions of the NP array, showing strong orientation of actin filaments in the ⟨10⟩ direction of the underlying NP array, while actin cytoskeletal organization had no preferred orientation on polished silicon (Figure 2D). Live imaging of membrane-dyed cells cultured at 1 day (Figure 2E) showed that at lower density cell elongation is pronounced and the morphological characteristics in live cells correspond with the SEM of the same cells, demonstrating the fidelity of the SEM preparation with respect to cell morphology and alignment with the NP array and that both live imaging and SEM studies can be used to assess the cell morphology. Figures 2E and S3 show the characteristic elongated morphologies of the cells and their preferred polarization in the ⟨10⟩ and ⟨11⟩ crystallographic directions of the underlying NP array.

To gain insight into the evolution of the unique morphologies of the cells on NPs, the early events of cell spreading were evaluated on live and fixed cells seeded on gradient pitch surfaces (Figure 3). Time-lapse microscopy on live cells with fluorescent lipophilic tracers was used to image the cell plasma membrane over the course of the first 60 min post-seeding. At 30 and 60 min post-seeding, the actin cytoskeleton was assessed by fluorescence staining, and morphology was assessed by SEM. Cells on polished silicon, 0.8 to 1 μm pitch and 1.5 to 2 μm pitch, each exhibited different morphological characteristics already 30 min post-seeding that were further accented at 60 min (Figure 3). At 30 min, cells on polished silicon extended lamellapodia-like sheets. Similar cell morphology was observed on 0.8 to 1 μm pitch NPs, with the addition of frequent short filopodia-like extensions oriented with the NP array. Notably, on 1.5 to 2 μm pitch NPs, broad lamellapodia-like extensions were infrequent and longer extensions protruded from the cell bodies, relative to cells on 0.8 to 1 μm pitch NPs. These characteristics were consistent for live cell imaging, actin staining, and SEM. Thus, within 30 min post-seeding cell morphology is already distinctly altered by the NP pitch. Cells were examined again at 60 min post-seeding, and these differences were more pronounced. At 60 min, cells were broadly spread on polished silicon and again had a similar morphology on 0.8 to 1 μm pitch NPs, but with short extensions oriented along the underlying NP array. In contrast, cells on 1.5 to 2 μm pitch NPs had substantially smaller projected areas and fewer, significantly longer extensions, developing into a distinctly polarized morphology at 60 min post-seeding.

Several additional surfaces were evaluated to further examine the parameters of the array that are responsible for cell polarization and alignment. These included (i) 1.5 μm diameter micropillars at a pitch of 3.5 μm fabricated to produce a similar gap distance between adjacent pillars to the 2 μm pitch NPs and

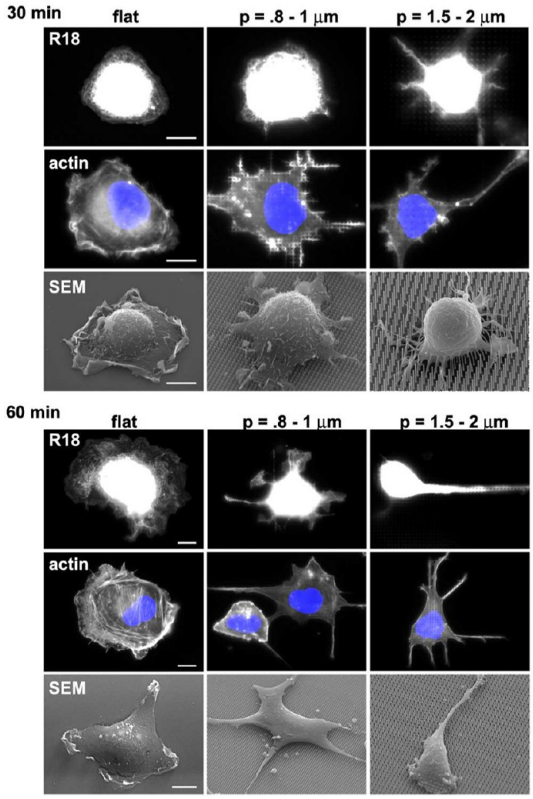

Figure 3. Early progression of cell spreading on NPs of varying pitch. At 30 min (top grid) or 60 min (bottom grid) post-seeding, R18-stained cells were first imaged live by fluorescence microscopy, then fixed, the actin cytoskeleton was optically imaged, and finally SEM images were taken. Images show representative cells on polished silicon (flat) and NP substrates. At 30 min post-seeding, cells on polished silicon and NPs with $p = 0.8-1.0\ \mu$m spread broadly and had less significant extensions compared to cells on NPs with $p = 1.5-2.0\ \mu$m. At 60 min, similar differences were apparent, and actin alignment with the NP grid primarily in the ⟨10⟩ direction was common on both ranges of NP spacings.

(ii) molded replicas of 2 μm pitch NPs (12:1 aspect ratio) in polymer (OG142, Epotek). Moreover, a variety of cell types were tested, including human mesenchymal stem cells, PC12 cells, and C3H10T1/2 cells. All cell types exhibited polarization and alignment on all of the substrates (Figure 4) in which the gap between pillars was at 1.6 to 2 μm spacing with some variance in the exact distance that elicits maximum polarization response for each cell type. Interestingly, PC12 cells grown on Si (Young's modulus of ~180 GPa) and epoxy (Young's modulus of ~1–2 GPa) showed similar morphology, suggesting that interpillar spacing may have a more significant role in inducing the specific morphological change, while the material's elasticity affects only the extent of cell polarization.

The axon-like morphology observed on 2 μm pitch NPs led us to evaluate the possibility that the surfaces were neural-inductive. Murine C3H10T1/2 cells were cultured on flat and 2 μm pitch, 50:1 aspect ratio NPs for 2 weeks in full serum and evaluated for βIII-tubulin

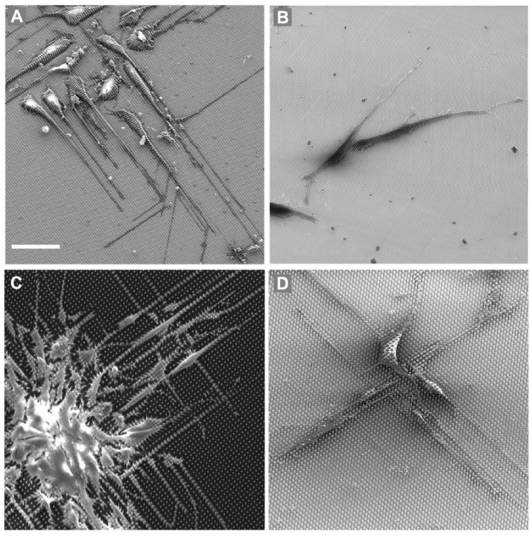

Figure 4. A variety of NP arrays with interpillar gaps of 1.6 to 2 μm all induce polarization of different cell types. In all studies cells were cultured for 1 day and imaged by SEM. (A) PC12 cells grown on high-aspect-ratio Si NPs (r = 100 nm, h = 10 μm, p = 2 μm), (B) human mesenchymal stem cells grown on Si NPs (r = 200 nm, h = 5 μm, p = 2 μm), (C) PC12 cells grown on an OG142 polymer micropillar array (r = 750 nm, h = 10 μm, p = 3.5 μm), and (D) C3H10T1/2 cells grown on a silicon micropost array (same topography as C) all exhibit similar cell body polarization and strong alignment with the ⟨10⟩ and ⟨11⟩ lattice directions. Scale bar 50 μm, magnification the same for all images.

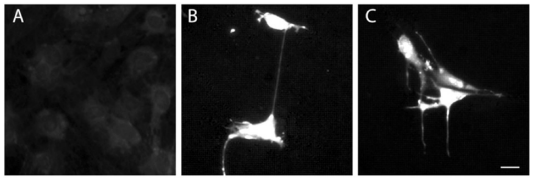

Figure 5. C3H10T1/2 cells immuno-stained for βIII-tubulin after 2-week culture on polished silicon (A) and NPs with $l = 10\ \mu$m, $r = 100$ nm, $p = 2\ \mu$m (B, C). βIII-Tubulin expression is higher in cells grown on high-aspect-ratio NP. Scale bar: 20 μm.

expression by immunohistochemistry. Cells on NPs stained more strongly for βIII-tubulin than control cells on flat Si (Figure 5), suggesting upregulation of the neuron-specific marker induced by culture on the NP array.

DISCUSSION

This study demonstrates the use of geometrically tunable nanopillar arrays to guide cell morphology by combinatorially varying the interpillar distance and NP aspect ratio. The results of stem cell growth on square arrays of cylindrical silicon NPs (with diameter 0.2–0.5 μm, height 5–10 μm, and interpillar spacings ranging from 0.8 to 5 μm) show that subtle changes in the NP spacing profoundly influence the projected area of the cells, cell body polarization, extension of cellular projections, and alignment of cell extensions with the NP grid. This transformation initiates quickly upon contact

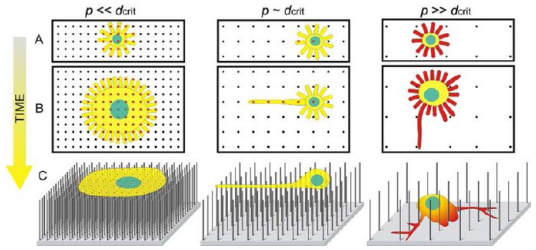

Figure 6. Schematic of the proposed cell spreading mechanism depicting the role of the spacing and symmetry of high-aspect-ratio NP arrays in controlling the morphology and alignment of stem cells. Red indicates areas of cell adhesion. Evolution of cell spreading at early (A) and late (B, C) stages of cell spreading. On high-density NP arrays where $p \ll d_{crit}$, the filopodia can establish focal adhesions with the surface in all directions. On medium-density NPs at distances between the NPs reaching d_{crit}, only extensions oriented in the ⟨10⟩ lattice directions will be able to find the adhesion, while extensions growing in other directions will be unable to bridge the gap > d_{crit}. On low-density NP arrays where $p \gg d_{crit}$, cells can no longer bridge the pillars in any direction; cells penetrate to the underlying substrate and extend at the floor of the nanoforest.

with the surfaces, with obvious differences in morphology becoming evident at 30 min post-seeding. Patterned arrays of adhesion sites on flat surfaces did not replicate these effects, indicating that the NP 3D topography, and not merely adhesion site restriction, accounts for our observations. Finally, we demonstrate the use of related topographies to produce similar effects, highlighting the importance of the interpillar gap in producing polarized, oriented cells, as well as use of molded polymeric NP arrays that can be applied to tissue engineering applications.

On the basis of the results of live imaging of the evolution of cell spreading (Figure 3) and comparison of the ensuing cell shapes (Figures 1, 2), we propose that, for a given cell type, a characteristic critical distance between NPs (d_{crit}) permits cells to bridge NPs as cell extensions elongate (Figure 6). For each cell type tested, the d_{crit} was close to 2 μm and shifted slightly dependent on the cell type, suggesting a common mechanism. For small interpillar distances (spacing less than 1.25 μm), the cells spread radially since they can reach posts for establishing the next focal adhesion contacts in all directions; as a result, the cells assumed a flattened morphology (Figure 6). With increasing NP spacing, extensions oriented with the NP lattice grow preferentially relative to those extending in directions not aligned with the lattice, where they have a higher probability of reaching the next post. Extensions preferentially grew in the ⟨10⟩ and ⟨11⟩ directions, *i.e.*, where the interpillar distances are shortest. When the lattice spacing reached d_{crit}, only cellular extensions aligned with the ⟨10⟩ can contact the next post to establish the focal adhesion (Figures 1, 2, Table 1). At a NP pitch of 2 μm, which corresponds to an interpillar gap, d_{crit}, of ~1.8 μm, the cell axis and extensions aligned with the ⟨10⟩ direction of the NP grid (Figure 2). At further increased interpillar distances (>3.5 μm), the cells no longer bridge the pillars and spread at the base of the NPs, resulting in increased branching of the extensions as bifurcations were formed around the NPs (Figure 1C).

The proposed mechanism provides a working model of cell interpretation of topography as a cue for growth and offers a basis for the rational design of NP arrays that can be optimized to program specific cell morphologies. In particular, we have demonstrated that the mode of cell spreading, rounding of the cell body, cell polarization, cell alignment, and branching of extensions can be switched on or off by tuning the order and availability of NPs for cell attachment. It is important to note that while the proposed mechanism emphasizes the role of NP spacing, the protein adsorption at the tips and the surface chemistry on the edges of these structures may also contribute.[53]

While others have identified strong polarization and alignment of cells on nanogrooved surfaces, they observed that these features were not prominent on NPs.[39] In contrast, our systematic, combinatorial study using high-aspect-ratio structures shows that such polarization is induced *only* at a characteristic interpillar distance near 2 μm, where NPs induced a rapid and marked cell polarization and alignment. The majority of cells showed growth of a single, small-diameter, axon-like process extending hundreds of micrometers and aligned with the underlying lattice. Control over such pronounced changes in stem cell shape have not been previously demonstrated on NPs, conceivably due the use of a different NP spacing and failure to appreciate the role such spacing has on the cell shape. Others have shown cell shape changes when adhesion site availability is defined by chemical patterning of 2D substrates.[5,11,15,31] We found that the extreme cell polarization and alignment observed in our study could not be replicated with 2D patterned adhesion sites that mimic the NP arrays and that the suspension of cells in the 3D geometry and the need to bridge the specific interpillar gaps are critical for the pronounced, directional cell polarization.

We observe increased βIII-tubulin immunostaining of C3H10T1/2 stem cells cultured on NPs spaced at 2 μm after 2 weeks in culture. While not a definitive marker for neural induction, it is consistent with other studies that have demonstrated neuronal induction by grooved nanostructures *via* topographic cues in the absence of serum withdrawal or addition of neurogenic agents.[24,54,55] Moreover, the observation that the extent of cell polarization and alignment increases with increasing NP aspect ratio is consistent with earlier studies showing neuronal induction of stem cells grown on flat, low-elastic-modulus materials.[56,57] These studies indicate that cells sense the substrate elasticity at the scale of focal adhesions.[11,14,55,58] An increase in NP aspect ratio leads to "geometrically

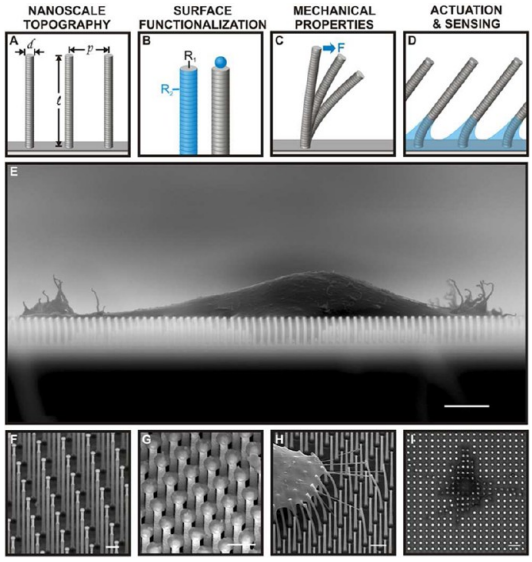

Figure 7. Proposed multifunctional nanopillar arrays for guiding cell behavior. (A) Nanotopographical cues are fabricated using NPs lithographically to provide specific geometry and spacing. (B) Asymmetric surface functionalization of the NPs can be used to specify cell adhesion sites and alter the wetting behavior of the surface. (C) The mechanical properties of NPs can be controlled by varying the geometry by photolithography/DRIE and bulk material properties. (D) Actuation of NPs can be used to stimulate cells or to detect forces exerted by cells on NPs. (E) SEM of stem cell growing on NP surface. (F) SEM of NP array. (G) SEM of NP tip functionalization with nanoparticles. (H) SEM showing the interaction of cells with the NPs, deflecting NPs. (I) Optical image of microposts bending under cellular forces.

softer" surfaces, which could lower the perceived stiffness of the substrate by the cell despite the high Young's modulus of the bulk material (note that a 2-fold increase in the aspect ratio results in a 10-fold decrease in the effective stiffness of the NPs). It is, therefore, likely that high-aspect-ratio NPs will undergo deflections under cellular forces and be perceived as elastic focal adhesions.[20] Such NP cantilevers can be expected to provide a potent mechanical stimulus to the cells and, thus, enhance the neurogenic potential of the substrate and possibly be engineered to mimic the nonlinear properties of protein matrices.[59]

While cytoskeletal rearrangement was reported to occur in astroglial cells seeded on low-aspect-ratio NPs,[24] these earlier studies have not shown either the remarkable morphological transformations or the alignment of the cellular processes that are observed in the current report. Our results strongly suggest that directional cytoskeletal rearrangement and subsequent specific changes in the stem cell shape are highly sensitive to minute variations in NP geometry and spacing. Further studies will be needed to substantiate whether the spacing-induced morphological changes correlate with differentiation and proliferation and the extent to which the geometry of NP surfaces alone can be used to specify, enhance, or accelerate stem cell differentiation, in particular to a neuronal type. Similar findings have been demonstrated in osteogenic differentiation using nanotopography alone.[60] In the present study, the ability to induce routine alignment of the cell extensions with the underlying lattice could be used to guide directional cellular junctions and, ultimately, their oriented growth into neural networks.

CONCLUSION

We envision that NP arrays can be further developed into a potent, multifunctional platform that synergistically coordinates topographical, chemical, and mechanical cues for cell guidance (Figure 7). The nanoscale topography can provide spatial cues for cell attachment;[43,47,48,51] the chemistry of the surface can be patterned to specify cell adhesion sites and provide directional signaling;[46,50] the NP mechanical properties can be tailored to mimic tissue matrix elasticity;[20,43] NP surfaces can be integrated with electronics for sensing and stimulating neuron signaling; and actuation of structures can be used to mechanically stimulate cells, dynamically alter topography,[45,49] or allow detection of forces exerted by cells. These nanobiomaterials offer a versatile platform in which the topography, surface chemistry, and physical properties of the NP arrays can each be tailored to manipulate cell behavior and to identify emergent cellular responses to combinatorial stimuli. Of particular importance is the ability to design these substrates to controllably reconfigure their geometry and therefore to provide a dynamic environment for cell growth.[45,49] Ongoing research will determine which combinations of specific NP arrangements, NP surface roughness, NP stiffness, actuation, and spatially defined chemistries are capable of guiding the growth and differentiation of stem cells. Such studies will offer further insight into how to design programmable materials for use in tissue engineering applications.

METHODS

Fabrication and Characterization of Nanopillar Arrays. Silicon NP arrays were fabricated by deep UV stepper lithography and Bosch deep reactive ion etching (DRIE) of single-crystal silicon wafers. A "gradient" sample was produced that included NP arrays with radius of 200 nm and height of 5 μm (aspect ratio of 12:1) arranged in a semicontinuous gradient of center-to-center interpillar spacings (pitch) from 0.8 to 5 μm. Surfaces with dedicated pitches of 1, 2, or 4 μm were also fabricated with 100 nm radius and 5 μm height. High-aspect-ratio structures were fabricated with a radius of 100 nm and height of 10 μm (aspect ratio of 50:1) set at a pitch of 2 μm. Additionally, micropillar surfaces were fabricated with 750 nm radius, 10 μm height, and 3.5 μm pitch. Surfaces were treated by oxygen plasma, and hydrophobic samples were prepared by silanization with (tridecafluoro-1,1,2,2-tetrahydrooctyl) trichlorosilane (Gelest, Inc. Morrisville, PA, USA). Polymeric

structures were produced by creating a PDMS mold of the silicon structure and casting as described previously using OG142 (Epotek, MA, USA).[43] The cantilever bending stiffness of the NPs was calculated using Young's modulus of silicon, the area moment of inertia based on the post geometry as measured by SEM, and assuming a force applied normal to the NP at its distal end. The cantilever stiffness of the NPs was confirmed by a direct measurement using AFM (Asylum Research, CA, USA).

Cell Culture. Cell lines studied included murine embryo-derived C3H10T1/2 cells,[52] primary human adult mesenchymal stem cells (hMSC) (obtained from Texas A&M Health Science Center College of Medicine), and murine pheochromocytoma cells (PC12).[61] Cells were cultured in alpha-MEM supplemented with L-glutamate (2 mM), penicillin (100 U/mL), and streptomycin (100 μg/mL) containing 10% heat-inactivated fetal bovine serum (FBS) (Fisher Scientific, USA) for C3H10T1/2 cells, 10% heat-inactivated horse serum plus 5% FBS for PC12 cells (16% horse serum), and 16.5% FBS for the hMSCs. Cells were expanded in 100 mm plastic culture dishes and subcultured prior to confluence. For all studies, low-passage cells were seeded from suspension in serum-free culture medium at concentrations of 5×10^4 to 5×10^6 cells/cm^2 and cultured. Hydrophobic substrates were force-wetted by pretreatment with 10 μL of 95% ethanol followed by a media exchange to wet the NPs prior to cell seeding. 2D arrays of adhesion sites mimicking the spacings of NP arrays were created by Au lift-off using the same lithographic masks used for NPs, producing arrays of Si dots on a Au background, followed by treatment with decanethiol and (3-aminopropyl)triethoxysilane (Sigma-Aldrich, MO, USA) to allow cells to adhere only to the aminated surfaces.[62] Immunohistochemistry was performed using rabbit anti-β-tubulin III primary, antineurofilament light chain, and fluorophore-labeled secondary antibodies (Sigma-Aldrich, MO, USA).

Microscopy and Analysis. Cell surfaces were rinsed in serum-free media and fixed with 2% glutaraldehyde in serum-free medium for 10 min followed by 2% glutaraldehyde in 0.1 M cacodylate buffer for 30 min. For SEM analysis, samples were then serial dehydrated in ethanol, critical point dried under CO_2 (Bal-Tec), Au sputter-coated, and imaged (JSM-5600LV) (JEOL 6350, JPN). For optical microscopy, fixed cells were stained with DAPI and rhodamine-phalloidin, and live cells were pretreated with R18 membrane dye (Invitrogen, CA, USA) prior to seeding, then imaged on a Leica DMRX microscope. Numerical analysis of cell morphological characteristics was performed using ImagePro (MediaCybernetics, MD, USA). Cell extensions were quantified by assessing the number of extensions greater than 20 μm in length per cell. Polarization was defined by cells with extensions longer than 50 μm. Directionality of cell growth was quantified by assessing the crystallographic direction that cell segments no wider than 2 μm bridged the NPs. Statistical analysis was performed by ANOVA with appropriate *post hoc* tests at the 0.05 level on the data sets (n = 3). Significant differences relative to p = 1 μm for 12:1 aspect ratio NPs and relative to polished silicon in 50:1 aspect ratio NPs are denoted with asterisks in the tables.

Conflict of Interest: The authors declare no competing financial interest.

Acknowledgment. This work was supported by the DOE under Award No. DE-SC0005247. We acknowledge the use of the facilities at the Harvard Center for Nanoscale Systems supported by NSF Award No. ECS-0335765. We would like to thank D. Ingber for fruitful discussions and A. Epstein for AFM work.

Supporting Information Available: SEM images of C3H10T1/2 and live cell fluorescence images of C3H10T1/2. This material is available free of charge *via* the Internet at http://pubs.acs.org.

REFERENCES AND NOTES

1. Ghosh, K.; Ingber, D. E. Micromechanical Control of Cell and Tissue Development: Implications for Tissue Engineering. *Adv. Drug Delivery Rev.* **2007**, *59*, 1306–1318.
2. Stevens, M. M.; George, J. H. Exploring and Engineering the Cell Surface Interface. *Science* **2005**, *310*, 1135–1138.
3. Langer, R.; Tirrell, D. A. Designing Materials for Biology and Medicine. *Nature* **2004**, *428*, 487–492.
4. Discher, D. E.; Mooney, D. J.; Zandstra, P. W. Growth Factors, Matrices, and Forces Combine and Control Stem Cells. *Science* **2009**, *324*, 1673–1677.
5. Vogel, V.; Sheetz, M. Local Force and Geometry Sensing Regulate Cell Functions. *Nat. Rev. Mol. Cell Biol.* **2006**, *7*, 265–275.
6. Silva, G. A.; Czeisler, C.; Niece, K. L.; Beniash, E.; Harrington, D. A.; Kessler, J. A.; Stupp, S. I. Selective Differentiation of Neural Progenitor Cells by High-Epitope Density Nanofibers. *Science* **2004**, *303*, 1352–1355.
7. Maloney, J. M.; Nikova, D.; Lautenschlager, F.; Clarke, E.; Langer, R.; Guck, J.; Van Vliet, K. J. Mesenchymal Stem Cell Mechanics from the Attached to the Suspended State. *Biophys. J.* **2010**, *99*, 2479–2487.
8. Hench, L. L.; Polak, J. M. Third-Generation Biomedical Materials. *Science* **2002**, *295*, 1014–1017.
9. Sniadecki, N.; Desai, R. A.; Ruiz, S. A.; Chen, C. S. Nanotechnology for Cell-Substrate Interactions. *Ann. Biomed. Eng.* **2006**, *34*, 59–74.
10. Yang, L.; Zhang, L.; Webster, T. J. Nanobiomaterials: State of the Art and Future Trends. *Adv. Eng. Mater.* **2011**, *13*, B197–B217.
11. Cavalcanti-Adam, E. A.; Volberg, T.; Micoulet, A.; Kessler, H.; Geiger, B.; Spatz, J. P. Cell Spreading and Focal Adhesion Dynamics are Regulated by Spacing of Integrin Ligands. *Biophys. J.* **2007**, *92*, 2964–2974.
12. Kunzler, T. P.; Huwiler, C.; Drobek, T.; Voros, J.; Spencer, N. D. Systematic Study of Osteoblast Response to Nanotopography by Means of Nanoparticle-Density Gradients. *Biomaterials* **2007**, *28*, 5000–5006.
13. Wen, X.; Cawthorn, W. P.; MacDougald, O. A.; Stupp, S. I.; Snead, M. L.; Zhou, Y. The Influence of Leucine-Rich Amelogenin Peptide on MSC Fate by Inducing Wnt10b Expression. *Biomaterials* **2011**, *32*, 6478–6486.
14. Discher, D. E.; Janmey, P.; Wang, Y. L. Tissue Cells Feel and Respond to the Stiffness of their Substrate. *Science* **2005**, *310*, 1139–1143.
15. Cherniavskaya, O.; Chen, C. J.; Heller, E.; Sun, E.; Provezano, J.; Kam, L.; Hone, J.; Sheetz, M. P.; Wind, S. J. Fabrication and Surface Chemistry of Nanoscale Bioarrays Designed for the Study of Cytoskeletal Protein Binding Interactions and Their Effect on Cell Motility. *J. Vac. Sci. Technol., B* **2005**, *23*, 2972–2978.
16. Geiger, B.; Bershadsky, A. Assembly and Mechanosensory Function of Focal Contacts. *Curr. Opin. Cell Biol.* **2001**, *13*, 584–592.
17. Geiger, B.; Bershadsky, A.; Pankov, R.; Yamada, K. M. Transmembrane Extracellular Matrix-Cytoskeleton Crosstalk. *Nat. Rev. Mol. Cell Biol.* **2001**, *2*, 793–805.
18. Tan, J. L.; Tien, J.; Pirone, D. M.; Gray, D. S.; Bhadriraju, K.; Chen, C. S. Cells Lying on a Bed of Microneedles: An Approach to Isolate Mechanical Force. *Proc. Natl. Acad. Sci. U. S. A.* **2003**, *100*, 1484–1489.
19. Kim, W.; Ng, J. K.; Kunitake, M. E.; Conklin, B. R.; Yang, P. D. Interfacing Silicon Nanowires with Mammalian Cells. *J. Am. Chem. Soc.* **2007**, *129*, 7228–7229.
20. Fu, J.; Wang, Y.-K.; Yang Mechanical Regulation of Cell Function with Geometrically Modulated Elastomeric Substrates. *Nat. Methods* **2010**, *7*, 733–736.
21. Curtis, A.; Wilkinson, C. Topographical Control of Cells. *Biomaterials* **1997**, *18*, 1573–1583.
22. Singhvi, R.; Stephanopoulos, G.; Wang, D. I. C. Effects of Substratum Morphology on Cell Physiology. *Biotechnol. Bioeng.* **1994**, *43*, 764–771.
23. Handarmin, H.; M., T.; Desai, R. A.; Yu, X.; Liu, Z.; Chen, C. S. Nanofibrous Scaffold with Incorporated Protein Gradient for Directing Neurite Outgrowth. *Drug Delivery Transl. Res.* **2011**, *1*, 147–160.
24. Turner, A. M. P.; Dowell, N.; Turner, S. W. P.; Kam, L.; Isaacson, M.; Turner, J. N.; Craighead, H. G.; Shain, W. Attachment of Astroglial Cells to Microfabricated Pillar Arrays of Different Geometries. *J. Biomed. Mater. Res.* **2000**, *51*, 430–441.

25. Ingber, D. E. Mechanical Control of Tissue Growth: Function Follows Form. *Proc. Natl. Acad. Sci. U. S. A.* **2005**, *102*, 11571–11572.
26. Kriparamanan, R.; Aswath, P.; Zhou, A.; Tang, L. P.; Nguyen, K. T. Nanotopography: Cellular Responses to Nanostructured Materials. *J. Nanosci. Nanotechnol.* **2006**, *6*, 1905–1919.
27. Curtis, A. S. G.; Dalby, M.; Gadegaard, N. Cell Signaling Arising from Nanotopography: Implications for Nanomedical Devices. *Nanomedicine* **2006**, *1*, 67–72.
28. Dalton, B. A.; Walboomers, X. F.; Dzieglielewski, M.; Evans, M. D.; Taylor, S.; Jansen, J. A.; Steele, J. G. Modulation of Epithelial Tissue and Cell Migration by Microgrooves. *J. Biomed. Mater. Res.* **2001**, *56*, 195–207.
29. Yang, M. T.; Sniadecki, N. J.; Chen, C. S. Geometric Considerations of Micro- to Nanoscale Elastomeric Post Arrays to Study Cellular Traction Forces. *Adv. Mater.* **2007**, *19*, 3119–3123.
30. Foley, J. D.; Grunwald, E. W.; Nealey, P. F.; Murphy, C. J. Cooperative Modulation of Neuritogenesis by PC12 Cells by Topography and Nerve Growth Factor. *Biomaterials* **2005**, *26*, 3639–3644.
31. Chen, C. S.; Mrksich, M.; Huang, S.; Whitesides, G. M.; Ingber, D. E. Geometric Control of Cell Life and Death. *Science* **1997**, *276*, 1425–1428.
32. Chou, L. S.; Firth, J. D.; Uitto, V. J.; Brunette, D. M. Substratum Surface-Topography Alters Cell-Shape and Regulates Fibronectin Messenger-RNA Level, Messenger-RNA Stability, Secretion and Assembly in Human Fibroblasts. *J. Cell Sci.* **1995**, *108*, 1563–1573.
33. Bissell, M. J.; Barcellos-Hoff, M. H. The Influence of Extracellular Matrix on Gene Expression: Is Structure the Message? *J. Cell Sci. Suppl.* **1987**, *8*, 327–343.
34. Teixeira, A. I.; Abrams, G. A.; Bertics, P. J.; Murphy, C. J.; Nealey, P. F. Epithelial Contact Guidance on Well-Defined Micro- and Nanostructured Substrates. *J. Cell Sci.* **2003**, *116*, 1881–1892.
35. Andersson, A. S.; Olsson, P.; Lidberg, U.; Sutherland, D. The Effects of Continuous and Discontinuous Groove Edges on Cell Shape and Alignment. *Exp. Cell Res.* **2003**, *288*, 177–188.
36. Kim, D. H.; Han, K.; Gupta, K.; Kwo, K. W.; Suh, K.-Y.; Levchenko, A. Mechanosensitivity of Fibroblast Cell Shape and Movement to Anisotropic Substratum Topography Gradients. *Biomaterials* **2009**, *30*, 5433–5444.
37. Biela, S. A.; Su, Y.; Spatz, J. P.; Kemkemer, R. Different Sensitivity of Human Endothelial Cells, Smooth Muscle Cells and Fibroblasts to Topography in the Nano-Micro Range. *Acta Biomater.* **2009**, *5*, 2460–2466.
38. Salem, A. K.; Searson, P. C.; Leong, K. W. Multifunctional Nanorods for Gene Delivery. *Nat. Mater.* **2003**, *2*, 668–671.
39. Choi, C. H.; Hagvall, S. H.; Wu, B. M.; Dunn, J. C. Y.; Beygui, R. E.; Kim, C. J. Cell Interaction with Three-Dimensional Sharp-Tip Nanotopography. *Biomaterials* **2007**, *28*, 1672–1679.
40. Zhao, Y.; Zhang, X. Cellular Mechanics Study in Cardiac Myocytes Using PDMS Pillars Array. *Sens. Actuators, A* **2006**, *125*, 398–404.
41. Sasoglu, F. M.; Bohl, A. J.; Layton, B. E. Design and Microfabrication of a High-Aspect-Ratio PDMS Microbeam Array for Parallel Nanonewton Force Measurement and Protein Printing. *J. Micromech. Microeng.* **2007**, *17*, 623–632.
42. Schmitz, G. J.; Brucker, C.; Jacobs, P. Manufacture of High-Aspect-Ratio Micro-Hair Sensor Arrays. *J. Micromech. Microeng.* **2005**, *15*, 1904–1910.
43. Pokroy, B.; Epstein, A. K.; Persson-Gulda, M. C. M.; Aizenberg, J. Fabrication of Bioinspired Actuated Nanostructures with Arbitrary Geometry and Stiffness. *Adv. Mater.* **2009**, *21*, 463–469.
44. Pokroy, B.; Kang, S. H.; Mahadevan, L.; Aizenberg, J. Self-Organization of a Mesoscale Bristle into Ordered, Hierarchical Helical Assemblies. *Science* **2009**, *323*, 237–240.
45. Sidorenko, A.; Krupenkin, T.; Taylor, A.; Fratzl, P.; Aizenberg, J. Reversible Switching of Hydrogel-Actuated Nanostructures into Complex Micropatterns. *Science* **2007**, *315*, 487–490.
46. Aizenberg, J.; Hatton, B. (President and Fellows of Harvard College, USA) Fluidics-Induced Localized Assembly of Materials Using a Superhydrophobic Surface Structure. U.S. Patent 12/745,207, Dec 1, 2008.
47. Kim, P.; Adorno-Martinez, W. E.; Khan, M.; Aizenberg, J. Enriching Libraries of High-Aspect-Ratio Micro- or Nanostructures by Rapid, Low-Cost, Benchtop Nanofabrication. *Nat. Protoc.* **2012**, *7*, 311–327.
48. Kim, P.; Epstein, A. K.; Khan, M.; Zarzar, L. D.; Lipomi, D. J.; Whitesides, G. M.; Aizenberg, J. Structural Transformation by Electrodeposition on Patterned Substrates (STEPS): A New Versatile Nanofabrication Method. *Nano Lett.* **2012**, *12*, 527–533.
49. Kim, P.; Zarzar, L. D.; Zhao, X.; Sidorenko, A.; Aizenberg, J. Microbristle in Gels: Toward All-Polymer Reconfigurable Hybrid Surfaces. *Soft Matter* **2010**, *6*, 750–755.
50. Vasquez, Y.; Fenton, E. M.; Chernow, V. F.; Aizenberg, J. Growth of Polygonal Rings and Wires of CuS on Structured Surfaces. *CrystEngComm* **2011**, *13*, 1077–1080.
51. Hochbaum, A. I.; Aizenberg, J. Bacteria Pattern Spontaneously on Periodic Nanostructure Arrays. *Nano Lett.* **2010**, *10*, 3717–3721.
52. Reznikof, C. A.; Brankow, D. W.; Heidelberger, C. Establishment and Characterization of a Cloned Line of C3H Mouse Embryo Cells Sensitive to Postconfluence Inhibition of Division. *Cancer Res.* **1973**, *33*, 3231–3238.
53. Johansson, F.; Carlberg, P.; Danielsen, N.; Montelius, L.; Kanje, M. Axonal Outgrowth on Nano-Imprinted Patterns. *Biomaterials* **2006**, *27*, 1251–1258.
54. Seidlits, S. K.; Lee, J. Y.; Schmidt, C. E. Nanostructured Scaffolds for Neural Applications. *Nanomedicine* **2008**, *3*, 183–199.
55. Engler, A. J.; Sen, S.; Sweeney, H. L.; Discher, D. E. Matrix Elasticity Directs Stem Cell Lineage Specification. *Cell* **2006**, *126*, 677–689.
56. Kim, S. H.; Lee, D.; Kang, Y. S. Recent Research Trends of Fibrin Gels for the Applications of Regenerative Medicine. *Tissue Eng. Regen. Med.* **2009**, *6*, 273–286.
57. Flanagan, L. A. C. A.; Ju, Y.-E.; Marg, B.; Osterfield, M.; Janmey, P. A. Neurite Branching on Deformable Substrates. *Neuroreport* **2002**, *13*, 2411–2415.
58. Sen, S.; Engler, A. J.; Discher, D. E. Matrix Strains Induced by Cells: Computing How Far Cells Can Feel. *Cell. Mol. Bioeng.* **2009**, *2*, 39–48.
59. Kang, H.; Wen, Q.; Janmey, P. A.; Tang, J. X.; Conti, E.; MacKintosh, F. C. Nonlinear Elasticity of Stiff Filament Networks: Strain Stiffening, Negative Normal Stress, and Filament Alignment in Fibrin Gels. *J. Phys. Chem. B* **2009**, *113*, 3799–3805.
60. Oh, S.; Brammer, K. S.; Li, Y. S. J.; Teng, D.; Engler, A. J.; Chien, S.; Jin, S. Stem Cell Fate Dictated Solely by Altered Nanotube Dimension. *Proc. Natl. Acad. Sci. U. S. A.* **2009**, *106*, 2130–2135.
61. Greene, L. A.; Tischler, A. S. Establishment of a Noradrenergic Clonal Line of Rat Adrenal Pheochromocytoma Cells which Respond to Nerve Growth Factor. *Proc. Natl. Acad. Sci. U. S. A.* **1976**, *73*, 2424–2428.
62. Spargo, B. J.; Testoff, M. A.; Nielsen, T. B.; Stenger, D. A.; Hickman, J. J.; Rudolph, A. S. Spatially Controlled Adhesion, Spreading, and Differentiation of Endothelial Cells on Self-Assembled Molecular Monolayers. *Proc. Natl. Acad. Sci. U. S. A.* **1994**, *91*, 11070–11074.